Journal of Magnetism and Magnetic Materials 481 (2019) 55–67

Contents lists available at ScienceDirect

Journal of Magnetism and Magnetic Materials

journal homepage: www.elsevier.com/locate/jmmm

Research articles

Magnetic characterisation of grain size and precipitate distribution by major and minor BH loop measurements

Jun Liu[a,*], John Wilson[b], Claire L. Davis[a], Anthony Peyton[b]

[a] Advanced Steel Research Centre, WMG, University of Warwick, Coventry CV4 7AL, UK
[b] School of Electrical and Electronic Engineering, University of Manchester, Manchester M13 9PL, UK

ARTICLE INFO

Keywords:
Ferritic steels
Magnetic properties
BH loop
Grain size distribution
Precipitate distribution

ABSTRACT

Grain size and precipitates have a significant effect on the mechanical properties of steels and it is desirable to be able to characterise these in a non-destructive manner. Grain and precipitate sizes and their spatial distributions in both an extra-low-carbon steel and a laboratory model steel have been individually varied and compared with a variety of characteristic magnetic parameters measured from major and minor magnetisation loops. These magnetic parameters are shown to be very sensitive to grain size distribution when there are no precipitates within the grains. However, the magnetic parameters exhibit complex behaviours with precipitate size distribution, which is linked to a critical precipitate size for effective pinning and another critical precipitate size for strongest pinning to domain walls. The interaction between grain size and precipitate distribution effects on the minor loop properties in the studied steels are discussed.

1. Introduction

Non-destructive evaluation (NDE) of steel microstructure using electromagnetic (EM) sensors can be used for process control during fabrication or damage monitoring in-service since microstructural features, such as grain size, phase balance, precipitation etc., affect the magnetic response. The use of the magnetisation (BH) curves, and in particular their major and minor loops, for the assessment and NDE of ferritic steels has gained increasing consideration over the past decade e.g. for inspection of cold rolling [1,2], creep [3] and degradation (fatigue) [4] in a range of steels. Whilst there has been significant work on developing empirical relationships between major/minor loop measurements and mechanical properties, it is invariably necessary to look at the microstructures in order to interpret and make better use of these relationships. The dependence of coercivity on grain size has long been reported to be an inverse linear or an inverse square root relationship, i.e. coercivity linearly increasing with the reciprocal of grain size or the reciprocal of the square root of grain size, based on experimental data [5,6] as well as theoretical calculation [7,8]. Landgraf et al. [6] reported generally inverse linear dependence for electrical steels and compared their results with the literature data. More interestingly, they took notice of the influence of the grain size distribution breadth, which had often been overlooked in the past, although recently modelling work has been reported for grain size distributions on low field permeability [9]. It is often beneficial to be able to characterise the microstructural feature distribution, as opposed to single microstructural parameters e.g. grain size distribution rather than average grain size, to give better understanding and prediction of the microstructure-property relationship.

Major/minor magnetisation loop measurements have proved sensitive to the distribution of microstructural features such as precipitates, grain boundaries and dislocations in complex microstructures, e.g. in power plant steels [10], and have the potential of being used to look at selected microstructural features of interest, for example, through minor loop measurements at different points within a larger magnetisation cycle by applying bias fields. More often than not, it is challenging to separate the effect of one type of microstructural feature from the other. For example, grain size effect may appear insignificant on some major loop properties i.e. coercivity or remanence when there are other microstructural features within grains (such as precipitates or dislocations) or there is a significant amount of second phase, as seen in some carbon or high-alloy steels [11,12]. However, even in these cases, grain boundaries are still expected to interact with the processes of domain wall (DW) movement or domain rotation. One may capture these effects by minor loop properties for a certain range of amplitudes or bias fields. In this paper, we have been able to vary and characterise grain size distributions and the precipitate distributions within the grains individually and establish a fundamental and quantitative link

* Corresponding author.
E-mail addresses: j.liu.2@warwick.ac.uk (J. Liu), john.wilson@manchester.ac.uk (J. Wilson), Claire.Davis@warwick.ac.uk (C.L. Davis), a.peyton@manchester.ac.uk (A. Peyton).

https://doi.org/10.1016/j.jmmm.2019.02.088
Received 30 November 2018; Received in revised form 25 February 2019; Accepted 26 February 2019
Available online 27 February 2019

Nomenclature

B_r^m	Minor remanence
B_r	Remanence
H_c^m	Minor coercivity
H_c	Coercivity
H_{fwhm}	Full width at half maximum of an incremental permeability peak
N_a	Number density of precipitates
W_h^m	Minor hysteresis loss
W_h	Hysteresis loss
ΔH	Minor loop amplitude
Φ	Total area fraction of precipitates
α_p	A parameter characterising the combined effects of precipitate size and interpartical spacing on coercivity
l_{nn}	Nearest neighbour spacing of precipitates
μ_Δ	Incremental permeability
$\mu_{\Delta_{max}}$	Maximum incremental permeability
μ_{ni}	Low-field or near-initial permeability
d_0	Critical precipitate size for effective pinning to domain walls
d_c	Critical precipitate size for the strongest pinning to domain walls
d_p	Precipitate size
$f_{pin_{max}}$	Maximum pinning strength to domain walls
f_{pin}	Pinning strength to domain walls
$\bar{d}_p$	Average precipitate size
$\hat{d}_p$	Mode of precipitate size distribution
$\widehat{H}_\Delta$	Incremental permeability peak position
$\bar{l}_{nn}$	Average nearest neighbour spacing of precipitates
CDF	Cumulative distribution function
CuLS	Laboratory steel featuring high Cu and S content
DW	Domain wall
ECD	Equivalent circular diameter
EDX	Energy Dispersive X-ray Spectroscopy
ELC	Extra low carbon
EM	Electromagnetic
FEM–SEM	Field Emission Gun Scanning Electron Microscopy
MFP	Mean free path
NDE	Non-destructive evaluation
PDF	Probability density function

between these two individual microstructural variables and the relevant magnetic properties by major and minor loop measurements. This fundamental study will help separate their individual effects, rather than inferred effects from complex microstructures, so as to facilitate the application of this technique to the NDE of selected microstructural features of interest.

2. Materials and experimental details

An extra low carbon (ELC) steel with 0.003 wt% C was normalised at 1000 °C, 1100 °C and 1200 °C for half an hour to obtain different grain size distributions. Three rod samples of 5 mm in diameter and 50 mm length in the different conditions, referred to as ELC–T1000, ELC–T1100 and ELC–T1200 respectively, were received from our partners (see Acknowledgement) together with the grain size data (equivalent circular diameter distributions) that had been obtained by Electron Backscatter Diffraction.

A *model* laboratory steel (referred to as CuLS), featuring high Cu and S and extra-low C content, was produced with a microstructure consisting of very coarse ferrite grains and many precipitates within the grains in the as-cast condition. The chemical composition of the steel is given in Table 1. A series of as-cast bar specimens measuring about 100 mm × 10 mm × 10 mm were made and then heat treated as described in Table 2 to vary the grain size and the precipitate distribution. Rod samples, 5 mm in diameter and 50 mm length, were machined for the hysteresis measurements. Metallographic samples were polished to a 0.05 µm finish with colloidal silica and then etched in 2% nital. Optical microscopy and Field Emission Gun Scanning Electron Microscopy (FEG–SEM) were used to characterise the microstructure. Grain boundaries in optical micrographs and outlines of precipitate particles in SEM micrographs were reconstructed using Image Pro Plus. The average length of diameters measured at 2° intervals passing through the object's centroid were taken as the equivalent circular diameter (ECD) of grains or particles. The nearest neighbour spacing between the precipitate particles were computed from the X and Y coordinates of the mass centre of the particles. Energy Dispersive X-ray Spectroscopy (EDX), equipped in FEG–SEM, were used to analyse the composition of the precipitates in the CuLS samples.

An in-house BH Analyser developed at the University of Manchester, described in [13], was used for BH loop measurement. A magnetic field was applied using a silicon-steel U-core with two excitation coils wrapped around the legs and driven by two power amplifiers fed with a low frequency time varying signal. The machined cylindrical sample was fitted into a slot in the core, to maximise coupling between core and sample. The axial applied field (H) was measured using a sensitive (0.16 mV/mAmT) Quantum Well Hall sensor, also developed at the University of Manchester. The axial flux density of the induced field (B) was measured using a 30-turn encircling coil connected to an instrumentation amplifier. A 1 Hz sinusoidal excitation was used for the measurement of the major loops and the minor loops without a bias field and 10 cycles were recorded and averaged.

Table 1
Chemical composition of the laboratory steel (wt%).

C	Cu	S	Mn	Si	Ni	N	P	Al	Ti
0.0023	0.5	0.034	0.21	0.011	0.5	0.001	0.001	0.002	0.0001

3. Microstructures

3.1. Extra low carbon steel

All the ELC samples have a simple microstructure consisting of only ferrite grains. Fig. 1 shows the different grain size probability distributions. The ELC–T1000 sample exhibits the narrowest size distribution amongst the three samples with an average grain size at 19 µm and a standard deviation of 11 µm and a mode at 14 µm. As the normalising temperature increases the grain size distributions broaden significantly. As a result, the average ECD grain size and the standard deviation approximately doubled for 1100 °C and doubled again for 1200 °C. The mode of ECD, however, increase less significantly, being approximately 21 µm and 38 µm for the 1100 °C and 1200 °C

Table 2
Heat treatment conditions.

Sample	Heat treatment condition
Ascast	As cast
1N5min	Normalising at 950 °C for 5 min
3N5min	Normalising at 950 °C for 5 min for three times
3N30min	3N5min + normalising at 950 °C for 30 min
3N3h	3N5min + normalising at 950 °C for 3 h
3N8h	3N5min + normalising at 950 °C for 8 h

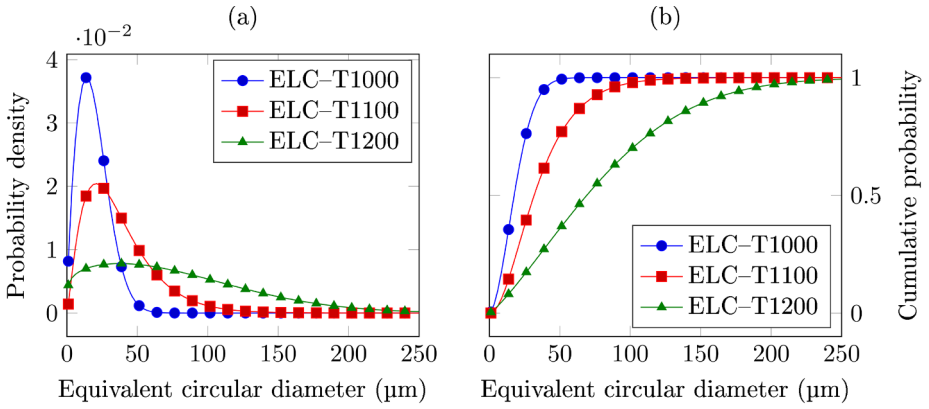

Fig. 1. Grain size distributions of the extra low carbon steel samples. (a) Probability density and (b) cumulative probability for equivalent circular diameter distributions.

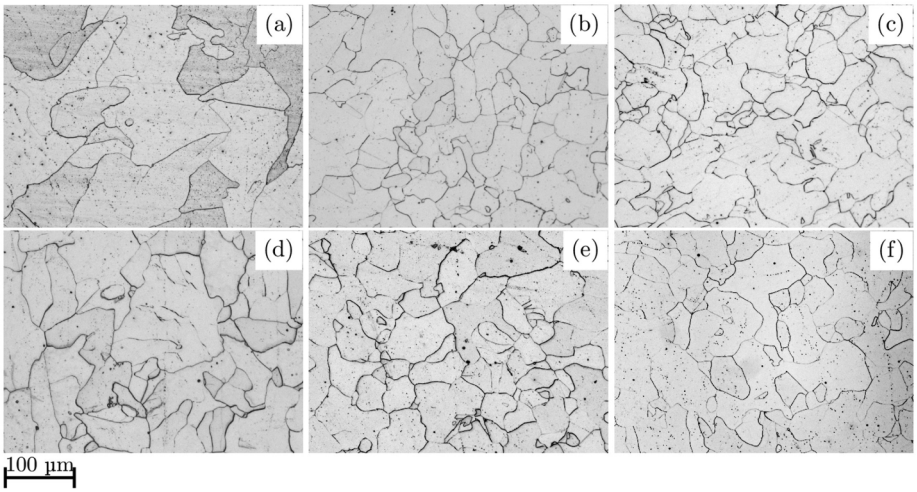

Fig. 2. Optical micrographs for the CuLS samples in the different conditions (a) as-cast, (b) 1N5min, (c) 3N5min, (d) 3N30min, (e) 3N3h and (f) 3N8h.

normalising respectively.

3.2. CuS-rich laboratory steel

Fig. 2 and Fig. 3 show the microstructures and the grain size distributions respectively for all the CuLS samples. The as-cast microstructure shows very coarse ferrite grains with a very broad size distribution (average size 162 ± 143 µm). Subsequent normalising heat treatments significantly refined the grains giving an average ECD grain size of approximately of 25–35 µm and a much narrower size distribution than the as-cast material. The grain size distributions for all the as-normalised samples are similar. Thus, the major microstructural differences between the as-normalised CuLS samples are the precipitate sizes and distributions.

Fig. 4 shows typical precipitates present in the as-cast sample including some very coarse (Mn,Cu)-S particles, with Cu-rich phase co-precipitating around them, as illustrated in the element mapping shown in Fig. 5, and many fine particles. The bi-modal precipitate size distribution is qualitatively in agreement with the literature e.g. [14,15]. The fine particles show significant variability in composition, particularly the S content: some particles are relatively rich in S, Mn and Cu with different (Mn + Cu):S ratio, collectively referred to as (Mn,Cu)-S; the other particles are either free of, or poor in, S (<0.01 at.%) and have similar EDX spectra as the matrix. These S-poor particles are, in general, slightly finer than the fine (Mn,Cu)-S ones. Fig. 6 plots the atomic percentage of (Mn + Cu) content as a function of that of S for a number of typical precipitates that are smaller than 0.5 µm in ECD for all the

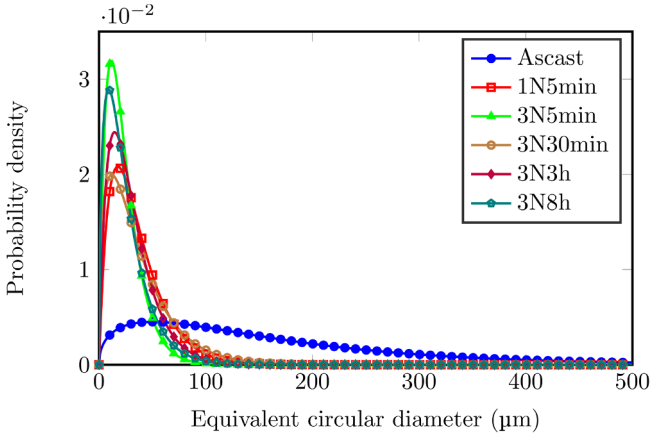

Fig. 3. Equivalent circular diameter distribution of ferrite grains for all the studied samples.

CuLS samples, with the colour of data points mapped to the precipitate size. The number density of the particles larger than 0.5 µm is two or three orders of magnitude lower than the finer precipitates. Their size and number do not change and hence any influence on the magnetic properties will remain constant in all the samples. Please note the S-free particles are excluded from Fig. 6 by the logarithm scale. A number of the (Mn,Cu)-S precipitates are identified as (Mn,Cu)S_{2-x} (where

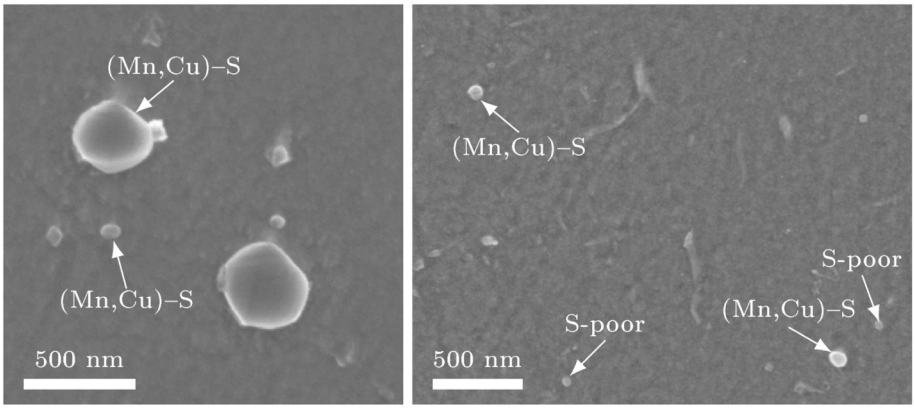

Fig. 4. Typical precipitates in the as-cast sample.

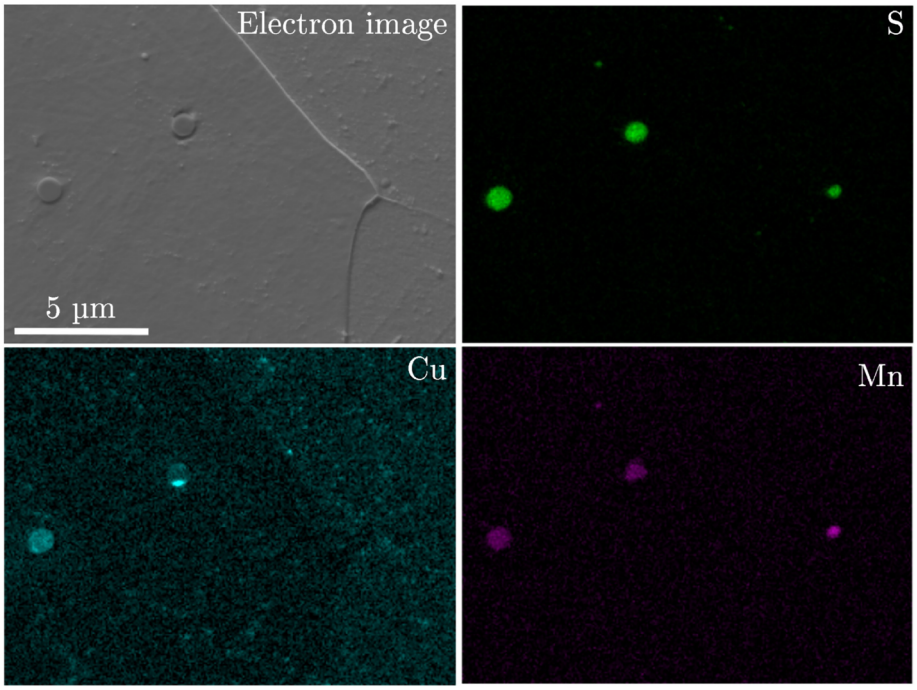

Fig. 5. Element mapping for S, Cu and Mn for the as cast sample.

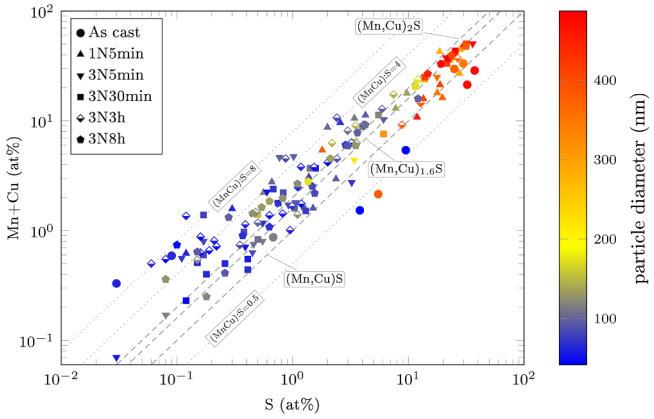

Fig. 6. The atomic percentage of (Mn + Cu) as a function of S of a number of typical precipitates (d_p < 500 nm) measured by EDX for all the CuLS steel samples. Fixed (Mn + Cu):S ratio of 1, 1.6 and 2, which are reported in the literature, are shown in dashed line whilst other ratios (dotted lines) are also plotted as assisting grid lines.

$0 < x < 1$), based on the fact that they occur around the (Mn + Cu):S= 0.5 trend line in Fig. 6 and also the literature [15] reporting fine (Mn,Cu)S_{2-x} particles found in similar as-cast (Cu,S)-rich low carbon steels. Neither these (Mn,Cu)S_{2-x} particles nor the S-free ones are detected in the as-normalised samples, which indicates they are metastable phases probably resulting from the fast kinetics of precipitation during casting. The coarse (Mn,Cu)-S particles formed in the solute-rich inter-dendritic region before final solidification and hence were able to grow very large. They are relatively stable and not expected to coarsen during the subsequent normalising heat treatments. In contrast, the fine particles, having precipitated at lower temperatures, are less stable and have coarsened during the normalising heat treatments, as can be observed in Fig. 7. The images have been intentionally selected to show the similar size of the large particles. The majority of the coarse particles (>0.5 µm) in the as-normalised samples are identified as (Mn,Cu) S or (Mn, $Cu)_{2-x}$S ($0 \leqslant x \leqslant 0.4$) according to the dashed lines for different (Mn + Cu):S ratios in Fig. 6, which is also in good agreement with the literature [15–18]. The finer particles (<200 nm) in the as-normalised samples, however, exhibit certain variability in the (Mn + Cu):S ratio, as can be observed in Fig. 6, and

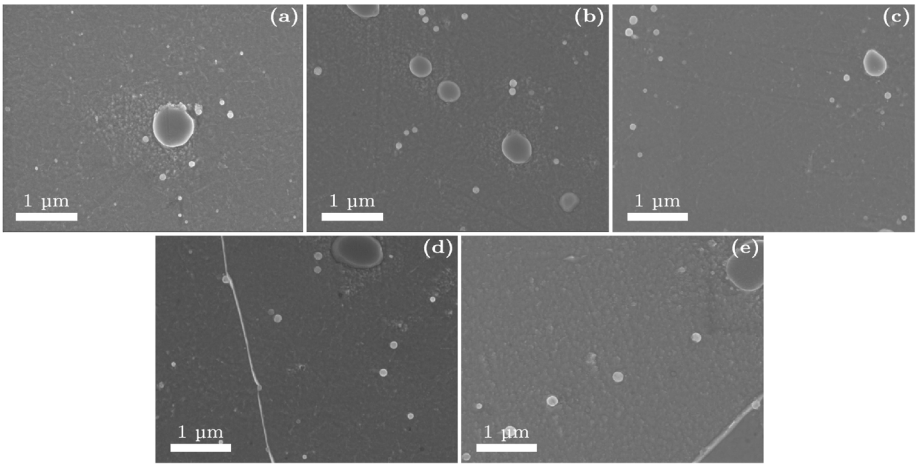

Fig. 7. Typical (Mn,Cu)-S precipitates (large, >0.5 µm, particles remain constant with heat treatment time and fine particles that coarsen with increased normalising time) in the as-normalised samples (a) 1N5min, (b) 3N5min, (c) 3N30min, (d) 3N3h and (e) 3N8h.

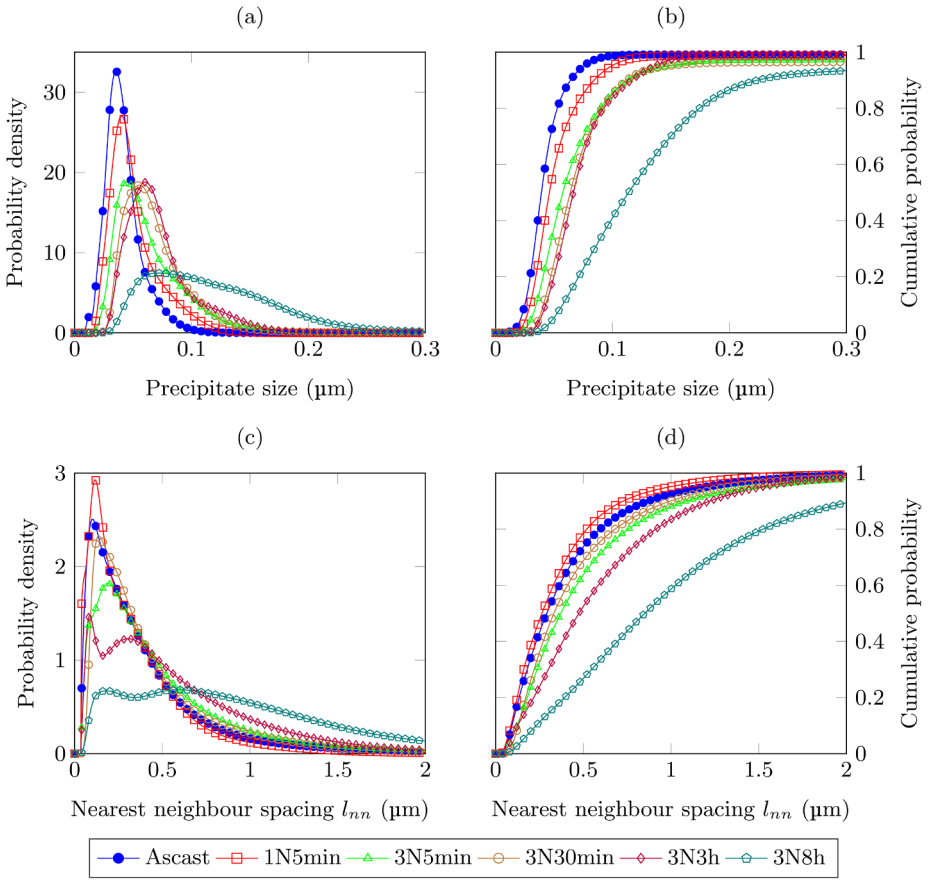

Fig. 8. Precipitate size and nearest neighbour spacing distributions. (a) probability density function (PDF) and (b) cumulative probability function (CDF) for precipitate size; (c) PDF and (d) CDF for nearest neighbour spacing distribution.

are also collectively referred to as (Mn,Cu)-S. Note that they are all non-magnetic and hence can be treated as the same type in terms of their pinning effects to DWs.

Fig. 8 shows the precipitate size (d_p) and inter-particle spacing (characterised as nearest neighbour spacing, referred to as l_{nn}) distributions in the form of a probability density function (PDF) and a cumulative distribution function (CDF) for the as-normalised samples. It should be noted that the very coarse (Mn,Cu)-S particles are too large and few in number to be shown on these distributions. There appears to be a very slight d_p broadening with insignificant change in l_{nn} distribution after a five-minute normalising (1N5min). It is therefore safe to say that major microstructural change between the as-cast and 1N5min samples is in the grain size distribution, as expected of such a short normalising heat treatment. There is a broadening of both d_p and l_{nn} from 1N5min to 3N5min, which indicates precipitate coarsening has occurred during the initial short multiple normalising cycles. In the next stage between the 3N5min and the 3N30min, d_p continues increasing whilst l_{nn} remains more or less constant. This would be consistent with the fine (Mn,Cu)-S precipitates growing larger by changing their composition, in particular enrichment of Mn [15], rather than coarsening by consuming their neighbours. There is again a significant broadening of both d_p and l_{nn} distribution after eight hours of normalising, which indicates coarsening

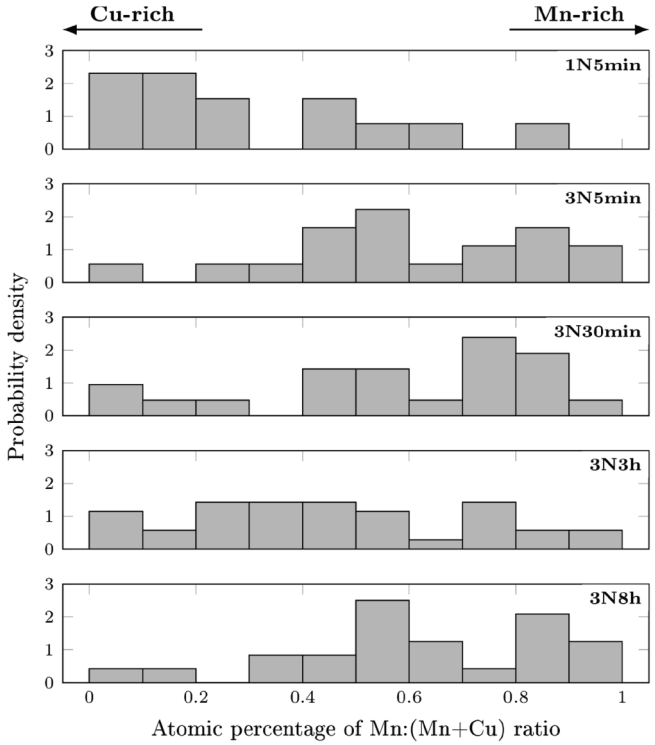

Fig. 9. Atomic percentage of Mn: (Mn + Cu) ratio distribution for the fine precipitates (<500 nm) in the as-normalised CuLS samples.

Table 3
Total area fraction (Φ) and number density per unit area (N_a) of the (Mn,Cu)-S precipitates in the laboratory steels.

	$\Phi(\times 10^{-3})$	$N_a(\times 10^{12}\mathrm{m}^{-2})$
Ascast	2.78 ± 1.00	1.55 ± 0.68
1N5min	3.59 ± 1.32	1.48 ± 0.45
3N5min	6.48 ± 3.42	0.83 ± 0.28
3N30min	5.82 ± 5.67	0.74 ± 0.33
3N3h	3.83 ± 0.47	0.76 ± 0.11
3N8h	10.66 ± 1.69	0.73 ± 0.21

is dominating as the (Mn,Cu)-S become compositionally stable. The 3N3h appears to be in the transition between an alloying-dominating (change in composition) and a coarsening-dominating stage, as indicated by the emergence of double peaks in the l_{nn} distribution, as can be seen in Fig. 8(c). These behaviours are evidenced by Fig. 9 showing the Mn: (Mn + Cu) ratio probability distribution for the fine precipitates smaller than 500 nm shifting from the Cu-rich region to the Mn-rich direction for normalising up to 3N30min; and, after eight hours of normalising, settling where Cu and Mn are more balanced near the Mn-rich region probably between 0.5 and 0.9 (Fig. 9); and at the same time where the (Mn + Cu):S ratio, in general, is converging to the more stable values between 1.6 and 2, as can be observed in Fig. 6.

The total area fraction (Φ) and number density per unit area (N_a) for the precipitates of $d_p \leq 0.5$ μm are given in Table 3.

4. Major and minor loop properties and their links to microstructures

4.1. Major loop properties and linkage to microstrutural parameters

4.1.1. Extra low carbon steels

Fig. 10 (a) shows the major loops for the ELC steel samples. It should be noted that the samples were magnetised to near technical saturation by applying a field of approximately 35 kA/m whilst only the [−5kA/m, 5kA/m] region is shown in Fig. 10 (a). The properties extracted from the major loops including coercivity, H_c, remanence, B_r, and hysteresis loss (the area encircled by a major loop), W_h, are given in Table 4. H_c values decrease with the average or mode of grain size by a power law with an exponent at approximately 0.5 or 0.15 respectively and a negative pre-exponent constant for the ELC steels, as shown in Fig. 10 (b), which is qualitatively in agreement with the literature [5,6] reporting H_c decreasing with average grain size also by a power law but with a different exponent at − 1 or − 0.5 and a positive pre-exponent constant. These empirical relationships as well as some theoretical predictions [8,7] are by no means universal. For example, Goodenough's [8] $1/d$ model fails for $d < 50$ μm, where d is average grain diameter; Landgraf's [6] $1/\sqrt{d}$ dependence, although valid for a broader range ($10 < d < 120$ μm) that covers the grain size range in this paper, was obtained using electrical steels with intra-grain precipitates present in all the samples and unavoidable texture in some of the samples. H_c is the applied field strength under which irreversible domain processes most frequently occur. Thus, it is fundamentally more logical to correlate H_c with the mode than the average of grain size. W_h, however, representing a cumulative result of all the irreversible domain processes over a major loop cycle, is collectively affected by all the grains and therefore should be correlated with the average grain size. The W_h values for the ELC samples decrease with the average grain size by a power law at an exponent of − 1.57 as shown in Fig. 10 (c). The B_r values are hardly distinguishable between the samples considering the scatter as can be seen in Fig. 10 (c) and Table 4.

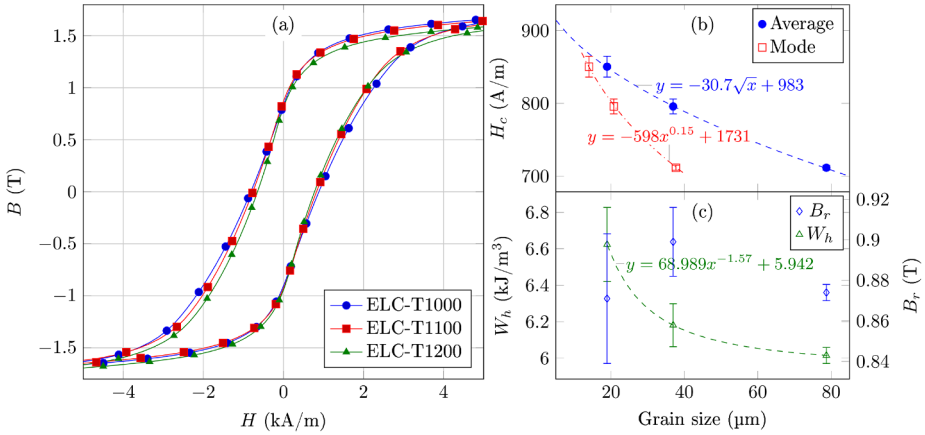

Fig. 10. (a) Major loops; (b) H_c and (c) W_h and B_r as a function of the grain size, for the extra low carbon steel samples. W_h and B_r are plotted against average grain size.

Table 4
Magnetic properties measured from the major and minor loops.

Sample	H_c (A/m)	B_r (T)	W_h (J/m^3)	$\mu_{\Delta max}$	$\widehat{H}_\Delta$ (A/m)	μ_{ni}	H_{fwhm} (A/m)
ELC–T1000	850 ± 14	0.871 ± 0.032	6624 ± 203	1210 ± 54	475 ± 39	433 ± 17	1786 ± 106
ELC–T1100	796 ± 10	0.899 ± 0.017	6181 ± 118	1475 ± 31	330 ± 19	514 ± 22	1378 ± 43
ELC–T1200	711 ± 3.5	0.874 ± 0.004	6015 ± 44	1781 ± 77	220 ± 10	595 ± 13	1081 ± 65
Ascast	657 ± 22	0.813 ± 0.034	5690 ± 226	1897 ± 49	192 ± 2	690 ± 24	1161 ± 34
1N5min	643 ± 5.4	0.808 ± 0.011	5501 ± 85	1670 ± 31	257 ± 20	552 ± 4	1241 ± 29
3N5min	638 ± 26	0.824 ± 0.010	5418 ± 179	1516 ± 28	266 ± 14	467 ± 15	1395 ± 54
3N30min	675 ± 16	0.853 ± 0.029	5693 ± 119	1487 ± 26	313 ± 15	435 ± 16	1473 ± 37
3N3h	690 ± 26	0.891 ± 0.027	5750 ± 185	1674 ± 27	321 ± 18	467 ± 20	1292 ± 27
3N8h	683 ± 8.8	0.846 ± 0.010	5626 ± 50	1587 ± 40	317 ± 7	478 ± 15	1398 ± 42

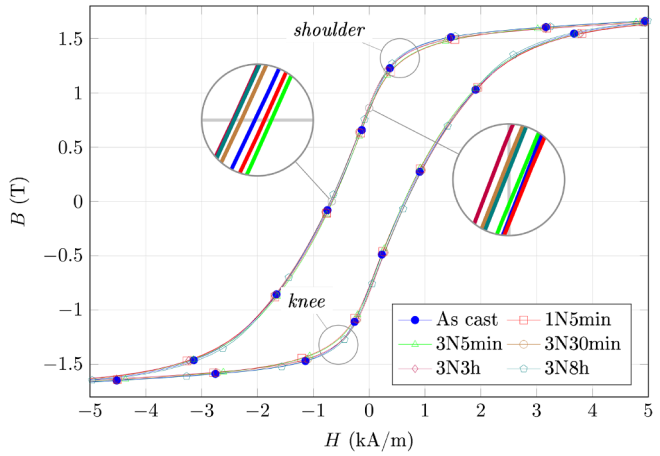

Fig. 11. Major loops for all the CuLS samples. The insets show the points of interest zoomed in.

4.1.2. CuS–rich laboratory steel

Fig. 11 shows major loops for all the CuLS samples. The extracted values of the major loop properties are given in Table 4. Despite significant difference in grain size distribution and similar precipitate distribution between the as-cast and the 1N5min sample, their major loop property values are very close. The loss of sensitivity to grain size distribution indicates that the precipitates play a more significant role in determining these properties when a significant number of them are present within the grains. Nevertheless, grain boundaries and grain orientations are still expected to affect the irreversible domain processes. The critical field associated with grains still contribute to the general critical field distribution and may affect the components associated with other microstructural features within the grains. We refer to this critical field as pinning strength f_{pin} for conciseness although it is not necessarily associated with a DW pinning event, more of a macroscopic descriptor of domain pinning effects. These complex effects cannot be explicitly captured by the major loop properties but may be characterised by minor loop measurements, which will be discussed later.

Non-magnetic intra-grain precipitates influence coercivity by pinning DWs due to DWs' strong tendency to stick to a precipitate to reduce the wall energy after Kersten [19] or due to the internal magnetic poles in a precipitate redistributing themselves when being passed by a DW to minimise magnetostatic energy after Neel [20]. Strongest pinning occurs where the precipitate size d_p is comparable with the DW thickness, which was reported to be around 120 nm in ferrite phase in carbon steels [21]. The number density of precipitates, N_a, also affects the pinning as a DW can be pinned by more than one precipitate at the same time. Combining both effects yields $H_c \propto \alpha_p \equiv N_a^{1/2} d_p^2$ following Kersten's model [19] or an empirical relationship reported in [22]. Fig. 12 shows a general trend of H_c and B_r initially increasing with coarsening of precipitates and then decreasing after a critical point around $\alpha_p \approx 3.5$ nm between 3N3h and 3N8h. The decrease of the H_c may be attributed to the fact that a significant number of precipitates has reached a critical size ≈ 120 nm i.e. comparable with the DW thickness, and hence their pinning effects start weakening with further coarsening. The initial increase of B_r is expected from the coarsening of precipitates reducing the number density of magnetic free poles and hence their contribution to demagnetisation; the latter decrease may be attributed to the fact that some of the precipitates have grown large enough (i.e. approximately ⩾ 200 nm [8], as seen in Fig. 8 for the 3N8h sample) for closure domains to form around them, which promotes demagnetisation and hence decreases B_r.

It has been shown that major loop properties are sensitive to an average or a total value of microstructural parameters, as opposed to a distribution, as a result of cumulative effects of all microstructural features. There may be an indication of microstructural feature distribution in the shape of a major loop, particularly near its *shoulder* or *knee* (Fig. 11). For example, a broad distribution of a high density of

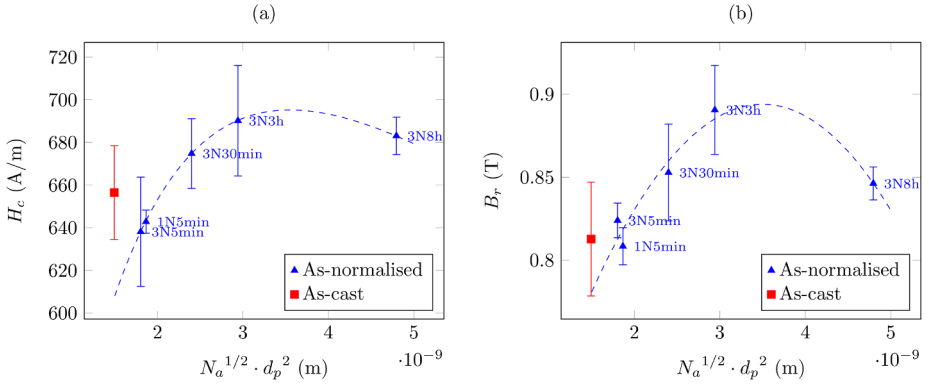

Fig. 12. Major loop properties (a) H_c and (b) B_r as a function of the number density (N_a) and size of precipitates (d_p) for all the CuLS samples. The error bars reflect the scatter for five repeated measurements.

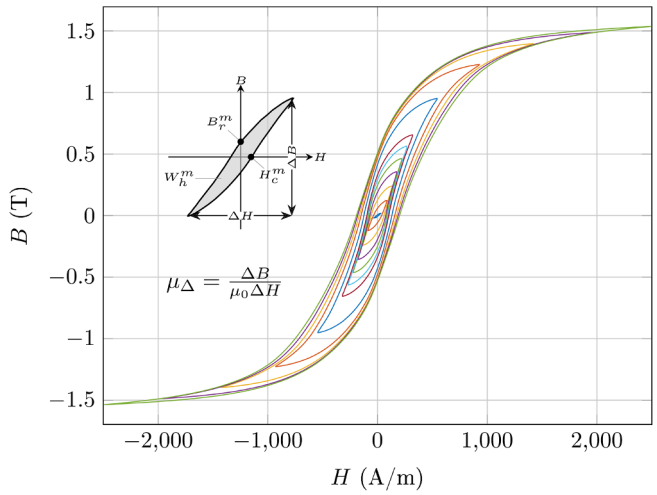

Fig. 13. A series of minor loops with different amplitudes.

dislocations within grains results in a rounded *shoulder* whilst recovery by annealing narrows the distribution of DW-pinning features and increases the major loop squareness [23]. However, such shape changes cannot be easily and quantitatively characterised. Besides, when there is more than one type of microstructural feature present, their effects on the major loop properties cannot be separated.

4.2. Minor loop properties and linkage to microstructural feature distributions

Fig. 13 shows a typical series of minor loops with increasing amplitudes. The inset illustrates the definition of a set of minor loop properties including incremental permeability μ_Δ, minor coercivity H_c^m, minor remanence B_r^m and minor hysteresis loss W_h^m, defined by analogy with their major loop counterpart to characterise the minor loop behaviours.

4.2.1. Extra low carbon steels

Fig. 14 shows the minor loop properties as a function of the minor loop amplitude for all the ELC samples. The μ_Δ profiles feature a single peak that can be characterised by its peak value, $\mu_{\Delta_{max}}$, peak position, $\widehat{H}_\Delta$, and the peak width at the half maximum, H_{fwhm} and they all fit well with a multi-term Gaussian function, as can be seen in Fig. 14 (a). The peaks occur approximately where the minor loops transit from a lenticular shape to a sigmoid shape typical of a major loop. Similar behaviours were previously reported on other ferromagnetic steels e.g. power plant P9 and T22 steels in different heat treated conditions [10]. The μ_Δ value at 35 A/m, approximately one thousandth of the major loop amplitude, was taken to characterise the low-field or near-initial permeability, referred to as μ_{ni}, as illustrated in Fig. 14 (a). The values of these characteristic parameters are given in Table 4. Fig. 15 shows these magnetic parameters as a function of corresponding microstructural parameters that characterise grain size distributions.

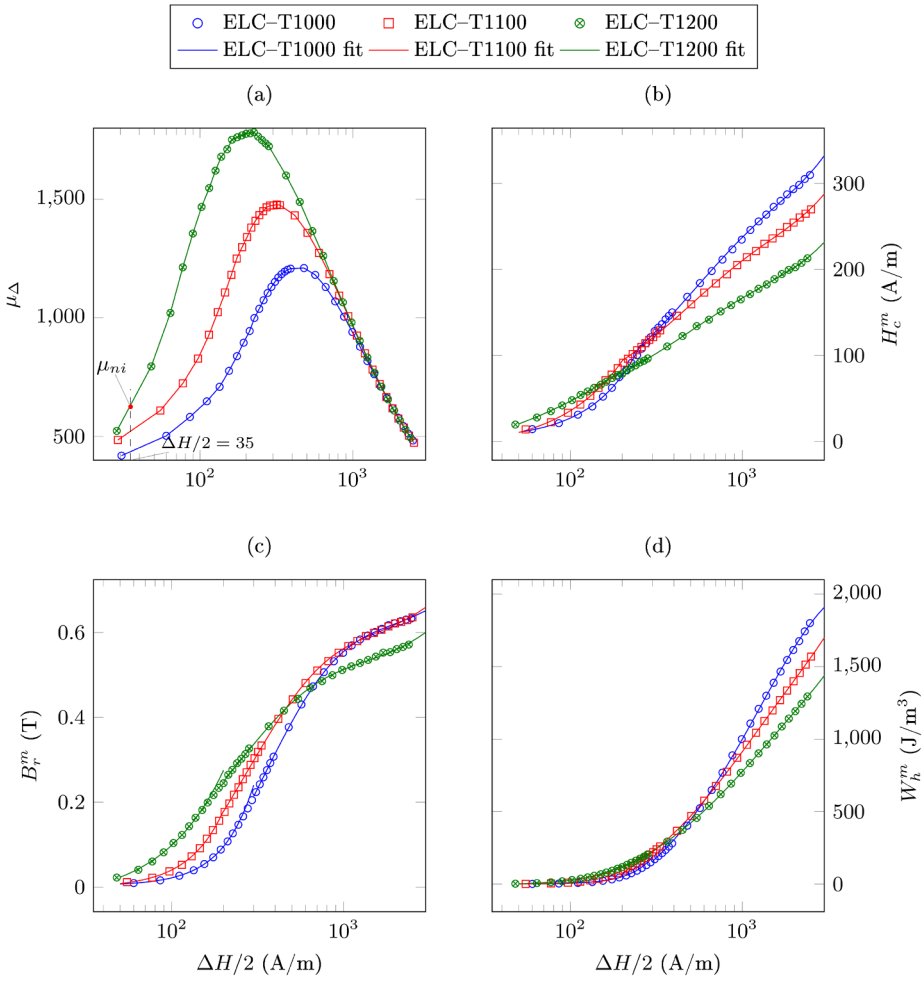

Fig. 14. Minor loop properties as a function of the minor loop amplitude for the extra low carbon steels. (a) μ_Δ, (b) H_c^m, (c) B_r^m and (d) W_h^m. The solid lines are fitting lines with multi-term Gaussian relationships in (a), power law and exponential relationships for low-amplitude portion and remainder of the curves respectively in (b), (c) and (d).

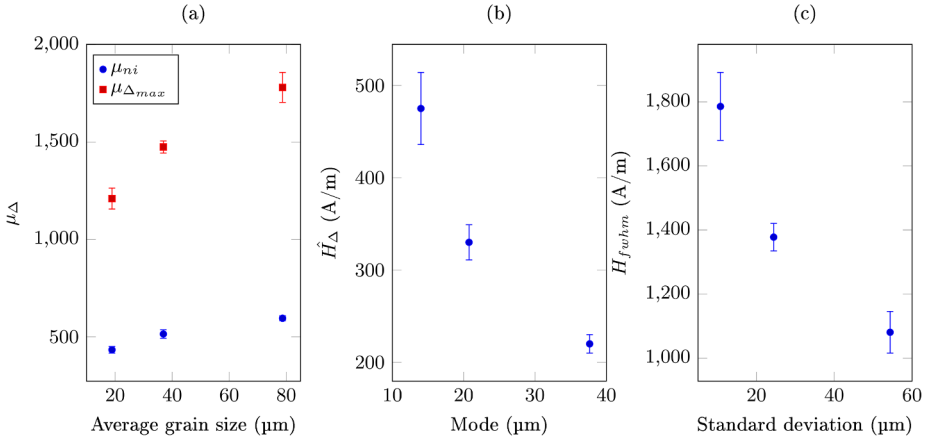

Fig. 15. μ_Δ profile parameters as a function of relevant grain size distribution parameters. (a) μ_{ni} and $\mu_{\Delta_{max}}$ as a function of the average grain size; (b) $\widehat{H}_\Delta$ as a function of the mode value of grain size; (c) H_{fwhm} as a function of the standard deviation of grain size.

Both μ_{ni} and $\mu_{\Delta_{max}}$ monotonically increase with average grain size. The latter shows a higher sensitivity than the former as can be observed in Fig. 15 (a). At very small amplitudes such as the one for μ_{ni}, predominant domain processes are 180° DWs oscillating between two equilibrium positions under the applied field of $-\Delta H/2$ and $\Delta H/2$ respectively. The oscillation can be translational motion or bending back and forth if the DW is treated as being rigid or flexible respectively. In either model, μ_{ni} is influenced by the mean free path (MFP) to DW motion, which is determined by the average grain diameters of all grains. As ΔH increases there will be increased coordination in the domain movement behaviours between some adjacent grains owing to the increased influence of the applied field, which effectively weakens the effect of the grain boundary as if these domains passed through the grain boundaries whose $f_{pin} < \Delta H/2$. These *passed* grain boundaries during minor loop cycles are not affecting μ_Δ any more. That is, μ_Δ is only sensitive to the grain boundaries that are effectively pinning DWs. Since f_{pin} is inversely proportional to grain size [8,7] those larger than a critical size, determined by the corresponding f_{pin}, are therefore separated out. It follows that μ_Δ is effectively sensitive to a truncated grain size distribution; an amplitude sweep is equivalent to truncating a grain size distribution from right to left (see Fig. 1 (a)). Note the probability density of a truncated distribution is scaled up. This accounts for a higher sensitivity of $\mu_{\Delta_{max}}$ than μ_{ni} to average grain size. $\widehat{H}_\Delta$ and H_{fwhm} decrease with the mode and standard deviation of the grain size distributions respectively as shown in Fig. 15 (b) and (c).

These behaviours and their consistency manifest a strong link between microstructural feature distributions (i.e. grain size distribution in this case) and incremental permeability profiles. The fundamental reason is that the latter can be mapped to the f_{pin} distribution, which has been explained in detail in our previous paper [10]. In short, the broader a grain size distribution the narrower its associated μ_Δ profiles (please note that the breadth of a μ_Δ profile is quantitatively characterised by its H_{fwhm} value in this paper). Thus, one can characterise grain size distribution using μ_Δ profiles by minor loop measurements.

Although the truncated portions of the grain size distribution are separated out in μ_Δ they are still actively affecting irreversible domain processes during a minor loop cycle and hence collectively effect the minor loop shape and other minor loop properties including H_c^m, B_r^m and W_h^m. Therefore, if these grains are of interest instead they can be characterised by these minor loop properties. For conciseness in describing their profiles, we divide the amplitude range roughly into three regions in terms of corresponding μ_Δ values. The region in which $\mu_\Delta \gtrsim \mu_{\Delta_{max}}/2$ is referred to as medium amplitudes; the region to the left and the right respectively is referred to as low and high amplitudes. In general, the trend of H_c^m, B_r^m and W_h^m changing with grain size inverses over the medium amplitudes. That is, at low amplitudes they all increase with grain size, whilst at high amplitudes they all exhibit a similar trend to their major loop counterparts. The low-amplitude portion fits well with a power law relationship, i.e. $y = a_1 x^{a_2} + a_3$ whilst the remaining curves fit well with a bi-exponential relationship i.e. $y = c_1\exp(c_2 x) + c_3\exp(c_4 x)$, where a_1, a_2, a_3 and c_1, c_2, c_3, c_4 are all constants independent of minor loop amplitude, as shown in Fig. 14 (b)–(d). The values of the constants for H_c^m are given in Table 5. All these constants show either a similar or inverse trend to the grain size distribution parameters. Similar to the f_{pin} distribution being mapped to μ_Δ profiles its cumulative distribution can be mapped to other minor property profiles since these properties reflect a cumulative result of the irreversible domain processes during a minor loop cycle. It follows that one can characterise the cumulative microstructural feature distribution using the H_c^m, B_r^m and W_h^m profiles. Instead of truncating the PDF of a grain size distribution, these properties are actually sampling grains by swiping the CDF from right to left. This explains why the low-amplitude values of these properties increase with average grain size because more grains in the broader distributions are sampled as can be observed in Fig. 1 (b). As the amplitude increases more grains are sampled at a rate similar to the tangent slope of the cumulative

Table 5
Fitting constants for the H_c^m profiles for all the studied samples.

	a_1	a_2	a_3	c_1	c_2	c_3	c_4
ELC–T1000	0.01836	1.568	2.052	2.3398E+02	1.1716E-04	−2.2759E+02	−2.1783E-03
ELC–T1100	0.1884	1.1899	−9.4861	2.0190E+02	1.1815E−04	−1.8120E+02	−2.3694E−−03
ELC–T1200	11.47	0.4628	−49.85	1.5596E+02	1.3183E−−04	−1.3139E+02	−2.4628E−−03
Ascast	2.211	0.6964	−11.73	1.3600E+02	1.1111E−−04	−1.1671E+02	−2.2219E−−03
1N5min	0.2041	1.1738	−2.5489	1.4656E+02	1.1774E−−04	−1.2603E+02	−2.7608E−−03
3N5min	0.0303	1.5518	1.9595	1.5808E+02	1.1978E−−04	−1.4454E+02	−3.0914E−−03
3N30min	0.0240	1.5758	3.1485	1.6613E+02	1.0419E−−04	−1.4546E+02	−2.5826E−−03
3N3h	0.0376	1.4818	2.2819	1.7039E+02	1.1310E−−04	−1.6799E+02	−3.1672E−−03
3N8h	0.0623	1.3840	1.2923	1.7498E+02	1.0553E−−04	−1.6549E+02	−2.7227E−−03

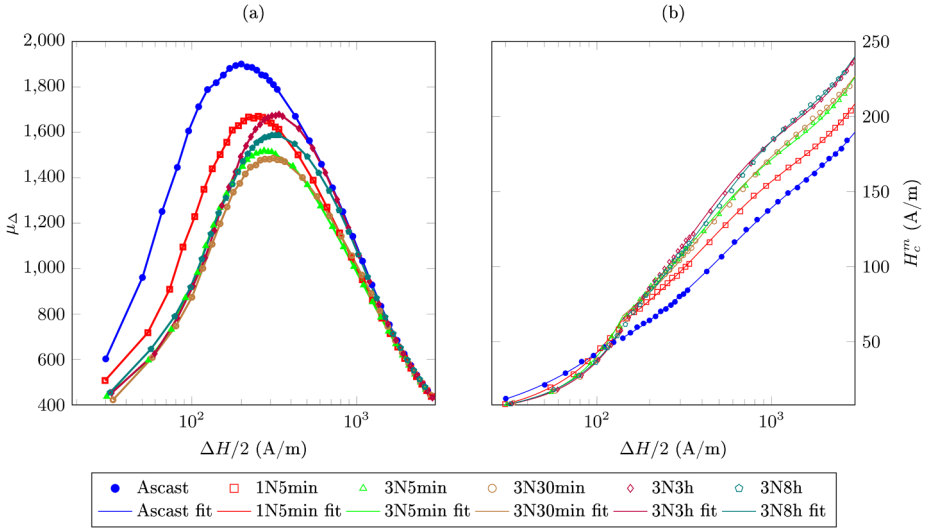

Fig. 16. Minor loop properties as a function of the minor loop amplitude for the CuS–rich laboratory steel. (a) μ_Δ; (b) H_c^m.

distribution profiles. That is, the broader the grain size distribution, the higher values these properties start with (at low amplitudes), and the lower the rates of increase with amplitudes. Eventually, the trend inverses.

4.2.2. CuS–rich laboratory steel

Fig. 16 shows the minor loop properties as a function of amplitudes for all the CuLS samples. Similarly, their μ_Δ profiles feature a single peak and H_c^m exhibit different behaviours between the low- and the high-amplitude region. The as-cast sample stands out with consistently greater μ_Δ values than the 1N5min sample for most of the amplitudes, the greatest $\mu_{\Delta_{max}}$ and the smallest $\widehat{H}_\Delta$ and H_{fwhm} (see Table 4), or in other words, the narrowest μ_Δ profile, amongst all the CuLS samples. There is continuous broadening of μ_Δ profiles for the as-normalised samples for normalising up to 30 min, indicated by a decreasing $\mu_{\Delta_{max}}$ and an increasing $\widehat{H}_\Delta$ and H_{fwhm}. Major changes occur over the low and medium amplitudes whilst the high-amplitude μ_Δ remain more or less constant in the stage between 1N5min and 3N30min. There is then a significant increase in $\mu_{\Delta_{max}}$ accompanied by a decrease in H_{fwhm}, or a narrowing of μ_Δ profiles, in 3N3h, but then again a broadening in 3N8h, with major changes occurring over the medium-high amplitudes in the next stage between 3N30min and 3N8h. However, $\widehat{H}_\Delta$ remains more or less constant in this stage.

Fig. 17 shows the μ_{ni} and the $\mu_{\Delta_{max}}$ values as a function of the mode or average value of precipitate size. μ_{ni} initially decreases with mode ($\widehat{d}_p$) or average value ($\bar{d}_p$) of precipitate size until they reach a minimum around 55 nm or 105 nm respectively, followed by a slower increase. The initial decrease of μ_{ni} can be attributed to a coarsening of the very fine precipitates that were too small to effectively pin DWs that turns them into effective pinning features, which results in a decrease in the MFP to DW motion. As a majority of precipitates become large enough to pin DWs, under the small amplitude for μ_{ni}, further coarsening consumes more DW-pinning precipitates than it turns into effective DW-pinning precipitates, which increases the MFP to DW motion, and hence μ_{ni} starts increasing. In short, the μ_{ni} behaviour indicates there is a critical precipitate size to a certain field, d_0, below which precipitates are not effectively pinning DWs. One may expect d_0 to have the following properties: (a) it should initially increase with the applied field; (b) it should be additive; that is, when many small precipitates are pinning DW together, d_0 should be considered as the equivalent size to their total area since the area intersecting with a DW (according to Kersten's theory) or the number of associated magnetic free poles (according to Neel's theory) are additive. Moreover, there is reportedly a critical precipitate size, d_c, where precipitates have strongest pinning strength to DWs; d_c was believed to be close to the Bloch wall thickness [21,24]. We map f_{pin} to precipitate size distribution as follows taking into account these behaviours:

1. As a first approximation, but not a necessary condition, we assume $f_{pin} \propto \exp(-A(d_p - d_c)^2)$ such that f_{pin} increases with d_p when

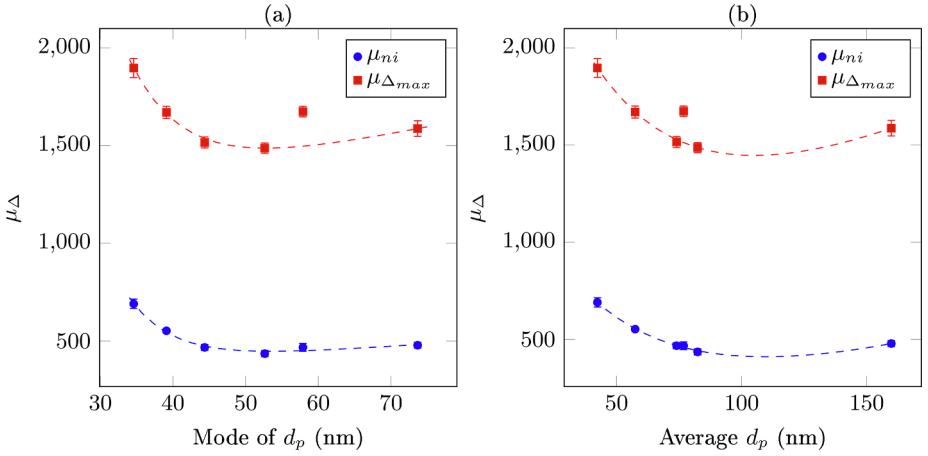

Fig. 17. Minor loop properties μ_{ni} and $\mu_{\Delta_{max}}$ as a function of precipitate distribution parameters (a) mode of d_p and (b) average d_p for all the CuLS samples.

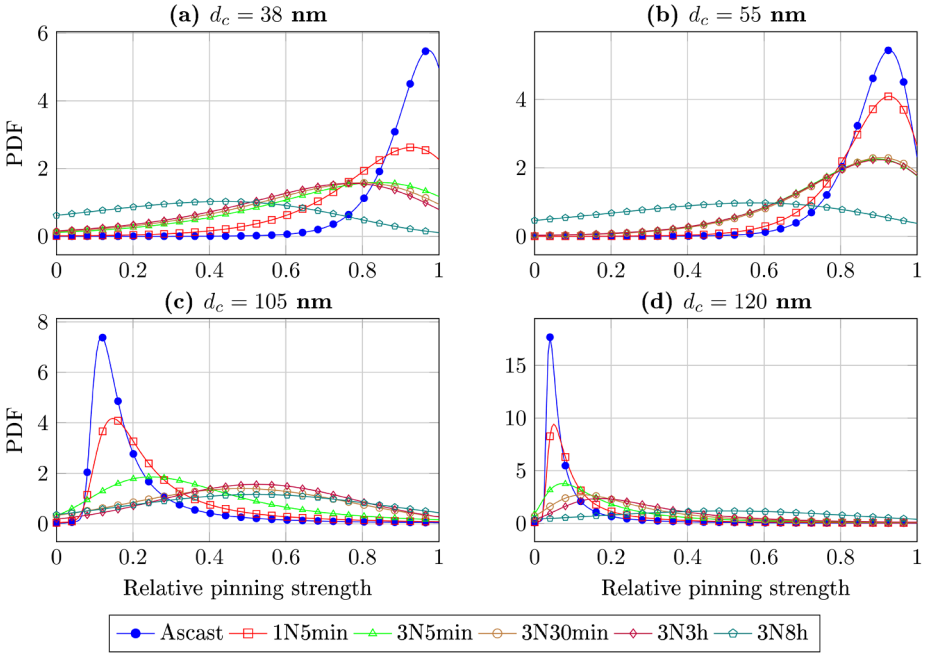

Fig. 18. Relative f_{pin} distribution for different critical precipitate size (d_c) for effective pinning to DWs. (a) 38 nm, (b) 55 nm, (c) 105 nm and (d) 120 nm.

$d_p < d_c$ until it reaches the maximum value that is normalised to unity by the exponential function when $d_p = d_c$, and then decreases when $d_p > d_c$. The pre-exponent constant A is to condition the f_{pin} values to distribute, overall, as broadly as possible between 0 and 1, for all the samples and different d_c values, which has been roughly determined to be in the range between 300 and 400, by trial and error.The trends for the peak positions and heights do not change with A in this range.

2. Map the relative f_{pin} distributions for different d_c values including a reported DW thickness for pure iron (38 nm) [25], the $\hat{d}_p$ and $\bar{d}_p$ value, where minimum μ_{ni} and $\mu_{\Delta_{max}}$ occur and a reported critical size (120 nm), for non-magnetic spherical cementite precipitates within ferrite grains in carbon steels, where maximum coercive force occurs [21].
3. Compare the trends for f_{pin} peak positions as a function of $\widehat{H}_\Delta$. As explained in our previous work [10] f_{pin} peak positions should be proportional to $\widehat{H}_\Delta$ and will be referred to as relative $\widehat{H}_\Delta$. However, $\mu_{\Delta_{max}}$ is affected by not only f_{pin} peak height (affecting how many DWs are moving) but also the interaction range (affecting how much the DWs move). The latter is influenced by inter-particle spacing distribution and grain size [10,26].
4. Assume$\mu_{\Delta_{max}} \propto f_{pin_{max}} \bar{l}_{nn}$ as a first approximation, where $f_{pin_{max}}$ is the f_{pin} peak height and $\bar{l}_{nn}$ is the average value of l_{nn} and the term on the right is referred to as relative $\mu_{\Delta_{max}}$. Compare the trends for relative $\mu_{\Delta_{max}}$ as a function of $\mu_{\Delta_{max}}$.
5. Re-sample the precipitates with $d_p \geqslant d_0$, where d_0 increases by 5 nm increments starting from 0, and update l_{nn}.
6. Repeat steps 1 to 5 until the trends are lost, which occurred at $d_0 = 35$ nm. Thus, the previous d_0, 30 nm, is regarded as the critical value for effective pinning the domain walls in these steels, which falls in the range (5–100 nm) for d_0 for iron reported in the literature [27].

Fig. 18 shows the relative f_{pin} distribution for different d_c values for $d_0 = 30$ nm. Fig. 19 shows relative $\widehat{H}_\Delta$ and relative $\mu_{\Delta_{max}}$ as a function of $\widehat{H}_\Delta$ and $\mu_{\Delta_{max}}$ respectively for the different d_c values. $d_c = 105$ nm yields best prediction to the expected trend as illustrated by the fitting line in Fig. 19. Note the value is comparable with the value (120 nm) for non-magnetic precipitates in carbon steels [21] and consistent with the μ_{ni}

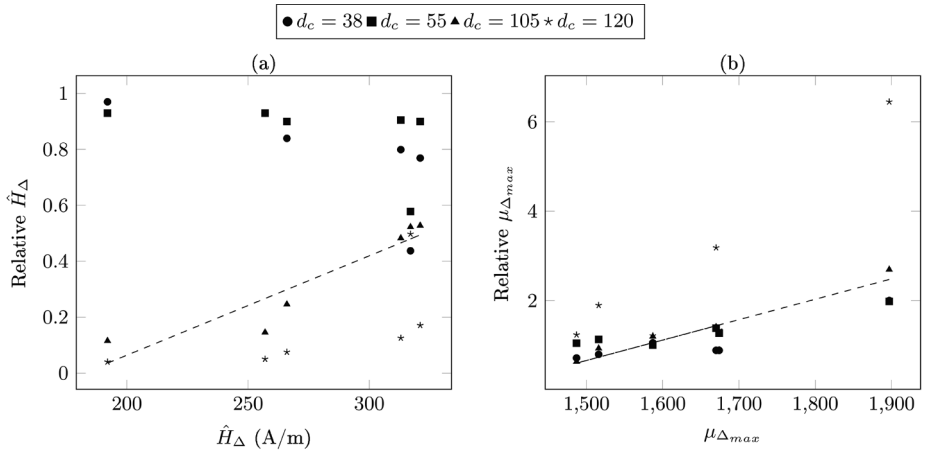

Fig. 19. (a) Relative $\widehat{H}_\Delta$ and (b) relative $\mu_{\Delta_{max}}$ as a function of $\widehat{H}_\Delta$ and $\mu_{\Delta_{max}}$, respectively. The dashed line shows a linear least-square fitting for the critical precipitate size $d_c = 105$ nm.

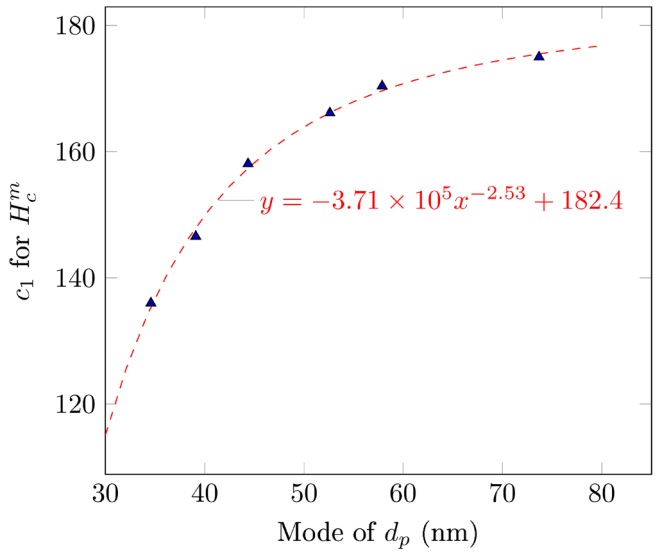

Fig. 20. H_c^m profile fitting constant as a function of the mode of d_p.

and $\mu_{\Delta_{max}}$ behaviours observed in Fig. 17 (b). As can be seen in Fig. 16 (a), the major difference between the 1N5min, 3N5min and 3N30min samples lies in the region to the left of the peak for 3N30min whilst the major difference between the 3N30min, 3N3h and 3N8h lies in the region to the right of peak for 3N30min. This accounts for the aforementioned similar μ_Δ behaviours as can be observed in Fig. 16. All the consistency indicates $d_c \approx 105$ nm for the CuLS steels.

The low-amplitude H_c^m are hardly distinguishable between the as-normalised CuLS samples as shown in Fig. 16 (b). The high-amplitude H_c^m start differing owing to a different rate of increase with amplitude as indicated by the fitting constants given in Table 5. Similar to the observed links to grain size distribution parameters for ELC samples, these fitting coefficients, independent of minor loop amplitude, are expected to be a function of precipitate distribution parameters. Fig. 20 shows the pre-exponent coefficient c_1 for the high-amplitude H_c^m increase with $\hat{d}_p$ fitting very well with a power law relationship. This fitting coefficient may be used to indicate the mode value for precipitate size. No strong link has been identified between the other coefficients and the precipitate distribution parameters probably due to the complexity of the underlying function and/ or scatter in the magnetic measurements and microstructural quantification. In the same spirit, Takahashi [1] and Kobayashi [3] first used some fitting coefficients between different minor properties, which are valid for a limited range of amplitudes, to indicate mechanical properties e.g. hardness and ductile–brittle transition temperature linked to dislocations in carbon steels and internal stress linked to Cu-rich precipitation in nucleation reactor pressure vessel steels. The present work sheds light on the underlying mechanism of this approach — the microstructural feature distribution governing the f_{pin} distribution and the interaction range after irreversible domain processes. Fundamental studies from first principles may be needed to fully understand the physical meaning of these coefficients.

5. Discussion on interaction between grain size effects and the precipitate effects

There is approximately 20% and 11% difference in μ_{ni} and $\mu_{\Delta_{max}}$ respectively between the as-cast and the 1N5min sample corresponding to a very slight d_p broadening but significant grain refinement. There is up to almost the same percentage of change in these magnetic properties between as-normalised CuLS samples corresponding to much more significant changes in precipitate distribution with similar grain size distribution. Thus, the significant difference in the μ_Δ profiles between the as-cast and the 1N5min sample (Fig. 16 (a)) should be principally attributed to grain size distribution (Fig. 3) effects. We have shown that grain size has strong influences on the μ_Δ profile when there are no precipitates or any other significant microstructural features within the grains as in the ELC samples. We shall then discuss what roles different grain size distributions play when there are similar distributions of precipitates present; and what roles the similar distributions of precipitates play when they are in grains of different size distributions.

Consider a 180° DW being pinned by precipitates in a grain. The origin of f_{pin} is twofold. First, the DW has to overcome the local potential wells associated with the precipitates. Second, DWs are subject to potential wells due to the magnetostatic energy associated with all the other grains of different orientations with the neighbouring grains having strongest influence. The smaller the grain size, the more grains with different orientations in a given volume there are and hence the deeper potential wells (higher f_{pin}) are to be overcome. It follows that grain size distribution can alter the f_{pin} distribution associated with the precipitates within grains. In contrast the other precipitates that are not pinning the DW are not expected to contribute much to the magnetostatic energy and hence the f_{pin} considering their small volume fraction. The shape of the f_{pin} distribution is dependent on the number density of local potential wells associated with precipitates, i.e. the number density of precipitates, and the number density of the potential wells associated with the grains. The typical 180° DW spacing for the CuLS samples, measured from the Bitter domain patterns without an applied field, as shown in Fig. 21, using the method described in [28], is in the order of several microns. It is worth noting that the Bitter pattern is on a 2D surface whilst the spacing in the 3D bulk may be different. However, it is still safe to say that the number density of DWs is estimated to be about three or four orders of magnitude lower than the number density of precipitates. In this case, the shape of the f_{pin} distribution will be

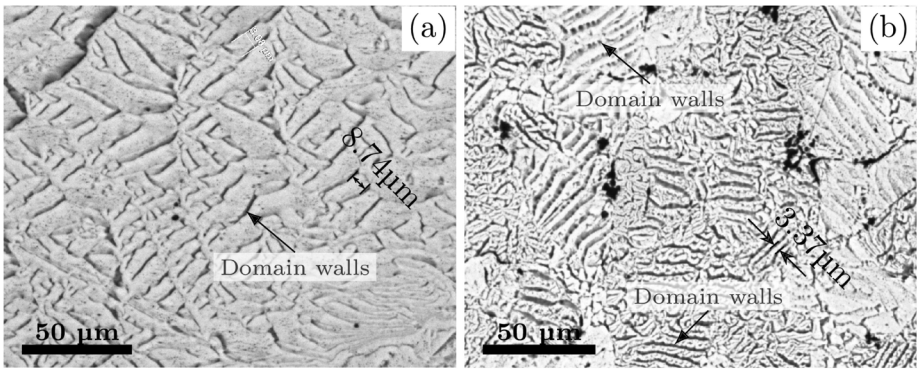

Fig. 21. Static domain patterns by Bitter method without an applied magnetic field for the (a) as-cast and (b) 1N5min CuLS steel samples. Examples of domain walls, shown as the dark line features, are marked and typical 180° domain wall spacings are measured.

dictated by the precipitate distribution whilst the predominant role of grain size distribution is to shift and scale the precipitate f_{pin} distribution. Therefore, narrower μ_{Δ} profile and smaller $\widehat{H}_{\Delta}$ of the as-cast sample than the 1N5min sample can be attributed to a larger and broader grain size distribution (and hence narrower associated f_{pin} distribution) of the as-cast sample shifting the f_{pin} distribution associated with precipitates to the left and at the same time making it narrower. In the meantime, the interaction range or the MFP to DW motion may be determined by grain size considering many precipitates may be too small to effectively pin DWs making the effective inter-particle spacing greater than the width of potential wells associated with grains. In this case or at high amplitudes, the MFP is grain size limited.

In the case of a very low number density of precipitates in a smaller and narrower grain size distribution (and hence higher number density of associated potential wells and broader f_{pin} distribution), the shape of the f_{pin} distribution may be dictated by the grain size distribution, whilst the precipitates are expected to play an insignificant role. The very coarse (Mn,Cu)-S particles have a very low number density and hence are expected to play an insignificant role in the shape of f_{pin} distribution.

6. Conclusion

Major loop properties including coercivity, H_c, and the hysteresis loss, W_h, are sensitive to grain size when there are no precipitates within the grains but become more or less insensitive to grain size when there are a significant number of precipitates within the grains. H_c and the remanence, B_r, show some sensitivity to average precipitate size and number density.

Characteristic magnetic properties/ parameters extracted from minor loops of a series of amplitudes including low field permeability, μ_{ni}, maximum incremental permeability, $\mu_{\Delta_{max}}$, and the amplitude where $\mu_{\Delta_{max}}$ occurs, $\widehat{H}_{\Delta}$, have proved sensitive to the grain size and precipitate distributions in the studied steels. The results indicate that there is a critical precipitate size, d_0, for effective pinning to domain walls that increases with the minor loop amplitude and there is another critical precipitate size, d_c, where the precipitates are most effectively pinning domain walls. d_0 and d_c were found to be approximately 30 nm and 105 nm respectively for the studied Cu-rich extra-low-carbon laboratory steels. The minor coercivity, minor remanence and minor hysteresis loss increase with the field amplitude by a power law at low amplitudes and a bi-exponential relationship at medium and high amplitudes. Some fitting coefficients exhibit strong links to grain size or precipitate size distribution parameters. It has been demonstrated that incremental permeability profiles and the fitting coefficients for the other minor property profiles can be used to indicate grain size and precipitate distributions.

Acknowledgement

The work was carried out with financial support from EPSRC under the Grant EP/K027956/2 with the CuLS steel being supplied by Tata Steel UK. The ELC samples were received from Tata Steel Europe and the heat treatments and grain size distributions were prepared by CEIT under an EU Research Fund for Coal and Steel grant RFSR-CT-2013-00031.

Appendix A. Supplementary data

Supplementary data associated with this article can be found, in the online version, athttps://doi.org/10.1016/j.jmmm.2019.02.088.

References

[1] S. Takahashi, S. Kobayashi, H. Kikuchi, Y. Kamada, Relationship between mechanical and magnetic properties in cold rolled low carbon steel, J. Appl. Phys. 100 (11) (2006) 113908, https://doi.org/10.1063/1.2401048.
[2] S. Takahashi, S. Kobayashi, H. Kikuchi, Y. Kamada, K. Ara, Analysis of minor hysteresis loops of cold rolled low carbon steel, IEEE Trans. Magn. 42 (11) (2006) 3782–3784, https://doi.org/10.1109/TMAG.2006.879147.
[3] S. Kobayashi, M. Tanaka, T. Kimura, Y. Kamada, H. Kikuchi, S. Takahashi, T. Ohtani, Changes of magnetic minor hysteresis loops during creep in Cr-Mo-V ferritic steel, J. Electr. Eng. 59 (7/s) (2008) 29–32 URL: http://iris.elf.stuba.sk/JEEEC/data/pdf/7s_108-08.pdf.
[4] L. Vandenbossche, L. Dupré, J. Melkebeek, Evaluating material degradation by the inspection of minor loop magnetic behavior using the moving preisach formalism, J. Appl. Phys. 99 (8) (2006) 08D907, https://doi.org/10.1063/1.2170960.
[5] J. Degauque, B. Astie, J. Porteseil, R. Vergne, Influence of the grain size on the magnetic and magnetomechanical properties of high-purity iron, J. Magn. Magn. Mater. 26 (1–3) (1982) 261–263, https://doi.org/10.1016/0304-8853(82)90166-4.
[6] F.J.G. Landgraf, J.R.F. da Silveira, D. Rodrigues-Jr, Determining the effect of grain size and maximum induction upon coercive field of electrical steels, J. Magn. Magn. Mater. (2011) 2335–2339, https://doi.org/10.1016/j.jmmm.2011.03.034 323(18–19).
[7] A. Mager, Über den Einflußder Korngröße auf die Koerzitivkraft, Ann. Phys. 446 (1) (1952) 15–16, https://doi.org/10.1002/andp.19524460104.
[8] J.B. Goodenough, A theory of domain creation and coercive force in polycrystalline ferromagnetics, Phys. Rev. 95 (4) (1954) 917–932, https://doi.org/10.1103/PhysRev. 95.917.
[9] L. Zhou, C. Davis, P. Kok, F. Van Den Berg, S. Labbé, A. Martinez-de Guerenu, D. Jorge-Badiola, I. Gutierrez, Magnetic NDT for steel microstructure characterisation – modelling the effect of ferrite grain size on magnetic properties, in: 19th World Conf. Non-Destructive Test. (WCNDT 2016), vol. 21, NDT.net, Munich, Germany, 2016. https://www.ndt.net/article/wcndt2016/papers/tu2h2.pdf.
[10] J. Liu, J. Wilson, M. Strangwood, C. Davis, A. Peyton, Magnetic characterisation of microstructural feature distribution in P9 and T22 steels by major and minor BH loop measurements, J. Magn. Magn. Mater. (2016), https://doi.org/10.1016/j.jmmm.2015.10.075.
[11] H. Kwun, G.L. Burkhardt, Effects of grain size, hardness, and stress on the magnetic hysteresis loops of ferromagnetic steels, J. Appl. Phys. 61 (4) (1987) 1576–1579, https://doi.org/10.1063/1.338093.
[12] D.C. Jiles, Magnetic properties and microstructure of AISI 1000 series carbon steels, J. Phys. D. Appl. Phys. 21 (7) (1988) 1186–1195, https://doi.org/10.1088/0022-3727/21/7/022.
[13] J. Wilson, N. Karimian, J. Liu, W. Yin, C. Davis, A. Peyton, Measurement of the magnetic properties of P9 and T22 steel taken from service in power station, J. Magn. Magn. Mater. 360 (2014) 52–58, https://doi.org/10.1016/j.jmmm.2014.01.057.
[14] Y. Ishiguro, K. Sato, T. Murayama, Precipitation of copper sulfide in ultra low carbon steel containing residual level of copper, Mater. Trans. 46 (4) (2005) 769–778, https://doi.org/10.2320/matertrans.46.769.
[15] B. Garbarz, J. Marcisz, Characterisation of dispersed nano-sulphides precipitated in low carbon steel solidified under high rate of cooling, Steel Res. Int. 79 (7) (2008) 523–529, https://doi.org/10.1002/srin.200806161.
[16] K. Urata, Y. Kobayashi, Formation of copper sulfide precipitate in solid iron, Adv. Molten Slags, Fluxes, Salts Proc. 10th Int. Conf. Molten Slags, Fluxes Salts 2016, Springer International Publishing, Cham, 2016, pp. 1229–1236, , https://doi.org/10.1007/978-3-319-48769-4_132.
[17] Z.Z. Liu, M. Kuwabara, B.H. Li, Y. Kobayashi, K. Nagai, Precipitation of copper sulfide and its effect on the microstructure and properties of steel, Steel Res. Int. 82 (5) (2011) 557–565, https://doi.org/10.1002/srin.201100037.
[18] Z. Liu, Y. Kobayashi, K. Nagai, Crystallography and precipitation kinetics of copper sulfide in strip casting low carbon steel, ISIJ Int. 44 (9) (2004) 1560–1567, https://doi.org/10.2355/isijinternational.44.1560.
[19] C. Kittel, Physical theory of ferromagnetic domains, Rev. Mod. Phys. 21 (4) (1949) 541–583, https://doi.org/10.1103/RevModPhys. 21.541.
[20] L. Neel, Effet des cavites et des inclusions sur le champ coercitif, Cah. Phys. 25 (1944) 21–44.
[21] L.J. Dijkstra, C. Wert, Effect of inclusions on coercive force of iron, Phys. Rev. 79 (6) (1950) 979–985, https://doi.org/10.1103/PhysRev.79.979.
[22] J.N. Mohapatra, Y. Kamada, H. Kikuchi, S. Kobayashi, J. Echigoya, D.G. Park, Y.M. Cheong, Effect of Cr-rich phase precipitation on magnetic and mechanical properties of Fe-20%Cr alloy, IEEE Trans. Magn. 47 (10) (2011) 4356–4359, https://doi.org/10.1109/TMAG.2011.2155047.
[23] A. Martínez-de-Guerenu, K. Gurruchaga, F. Arizti, Use of magnetic techniques for characterisation of the microstructure evolution during the annealing of low carbon steels, 9th European Conference on Non-Destructive Testing (ECNDT 2006), Berlin, Germany, 2006 p. Mo.2.2.2..
[24] D.J. Buttle, J.P. Jakubovics, G.D. Briggs, C.B. Scruby, Magneto-acoustic and barkhausen emission from domain-wall interactions with precipitates in incoloy 904, Philos. Mag. A 55 (6) (1987) 735–756, https://doi.org/10.1080/01418618708214380.
[25] D. Jiles, Introduction to Magnetism and Magnetic Materials, 2nd edition, Chapman and Hall, London, 1998.
[26] C.C.H. Lo, Modeling the effects of nanosized precipitates on magnetic hysteresis and barkhausen effect signal, J. Appl. Phys. 111 (7) (2012) 07D109, https://doi.org/10.1063/1.3672403.
[27] P. Gaunt, Magnetic coercivity, Can. J. Phys. 65 (10) (1987) 1194–1199, https://doi.org/10.1139/p87-195.
[28] J. Liu, J. Wilson, C. Davis, A. Peyton, Optimized setup and protocol for magnetic domain imaging with in situ hysteresis measurement, J. Vis. Exp. 129 (2017), https://doi.org/10.3791/56376.